Wave-related Reynolds number parameterizations of CO_2 and DMS transfer velocities

Sophia E. Brumer[1], Christopher J. Zappa[1], Byron W. Blomquist[2,3], Christopher W. Fairall[2], Alejandro Cifuentes-Lorenzen[4], James B. Edson[4], Ian M. Brooks[5], and Barry J. Huebert[6]

[1] Ocean and Climate Physics Division, Lamont-Doherty Earth Observatory, Columbia University, Palisades, NY, USA

[2] National Oceanic and Atmospheric Association, Earth Systems Research Laboratory, Boulder, CO, USA

[3] Cooperative Institute for Research in Environmental Sciences (CIRES), University of Colorado, Boulder, CO, USA

[4] Department of Marine Sciences, University of Connecticut, Groton, Connecticut

[5] School of Earth and Environment, University of Leeds, Leeds, UK

[6] Department of Oceanography, University of Hawaii, Honolulu, HI, USA

Corresponding Author: Sophia E. Brumer, Ocean and Climate Physics Division, Lamont-Doherty Earth Observatory, Columbia University, 61 Route 9W, Palisades, NY 10964, USA, sbrumer@ldeo.columbia.edu

Submitted: July 25, 2017

Revised: September 4, 2017

Abstract

Predicting future climate hinges on our understanding of, and ability to quantify air-sea gas transfer. The latter relies on parameterizations of the gas transfer velocity k, which represents physical mass transfer mechanisms and is usually parameterized as a non-linear function of wind forcing. In an attempt to reduce uncertainties in k, this study explores empirical parameterizations that incorporate both wind speed and sea state dependence via wave-wind and breaking Reynolds numbers, R_H and R_B. Analysis of concurrent eddy covariance gas transfer and measured wave field statistics supplemented by wave model hindcasts shows for the first time that wave-related Reynold numbers collapse four open ocean datasets that have a wind speed dependence of CO_2 transfer velocity ranging from lower than quadratic to cubic. Wave-related Reynolds number and wind speed show comparable performance for parametrizing DMS which, because of its higher solubility, is less affected by bubble-mediated exchange associated with wave breaking.

1. Introduction

In the current age of anthropogenic climate change, it is imperative to reduce uncertainties in climate predictions to allow for sound mitigation guidelines. Adequate characterization of gas transfer across the air-sea interface is not only essential to quantify local and global sinks and sources of carbon dioxide, CO_2, but also to budget many other trace gases that influence Earth's climate [*Carpenter et al.*, 2012]. These include, amongst others, marine aerosol precursors such as dimethyl sulfide, DMS [*Charlson et al.*, 1987].

The bulk gas flux (F_x) across the air-sea interface can be expressed as a function of the concentration difference (ΔC_x) across the air-water interface, and a kinematic parameter, the transfer velocity (k_x):

$$F_x = k_x \Delta C_x = k_x \alpha_x (p_{xw} - p_{xa}), \quad (1)$$

where α_x is the solubility of the gas, x, in seawater, p_{xa} and p_{xw} are the partial pressures of x in the air and surface water, respectively. k_x represents the mass transfer resistances of various physical forcing mechanisms and incorporates the dependence of the transfer on the diffusivity of the gas in water (which varies for different gases, temperatures and salinities).

Studies have shown that the interfacial transfer velocity is regulated by the turbulence in the air and water surface microlayers, which arises from wind stress at the water surface and buoyancy effects [*Jähne et al.*, 1987; *Komori et al.*, 1993]. k is therefore typically parameterized as a function of wind speed (U). One of the earliest parameterizations [*Liss and Merlivat*, 1986] derived from various field and laboratory measurements was a three piece linear function of U, corresponding to wind regimes in which no waves, capillary waves, or breaking waves are present. For simplicity and practical reasons, the impacts of waves were later ignored and a single quadratic [*Wanninkhof*, 1992] or cubic [*McGillis et al.*, 2001; *Wanninkhof and McGillis*, 1999a; b] function linking k to U were adopted for all sea states.

Current climate modeling studies most commonly use quadratic wind speed parameterizations for k *[Arora et al., 2013; Wanninkhof, 1992]*. These parameterizations are tuned to give the correct result for the global radiocarbon carbon budget over yearly or decadal timescales [*Sweeney et al.*, 2007; *Wanninkhof*, 1992; 2014] and provide an important constraint for global studies, but have an uncertain relationship to transfer mechanisms over limited temporal and spatial scales. Recent eddy-covariance measurements [*Garbe et al.*, 2014] highlight the inadequacy of wind speed only parameterizations for gas transfer velocities. For wind speeds above 10 m s^{-1} observations display substantial scatter and wind speed dependent parameterizations diverge; this can be attributed to a variety of environmental conditions and processes, mainly associated with surface waves. The complex interplay of these processes means that wind speed alone cannot capture the variability of air-water gas exchange. For winds over 7 m s^{-1}, breaking waves become a key factor to consider when estimating gas fluxes. Both theoretical and experimental studies suggest that wind waves and their breaking can significantly enhance gas exchange [*Woolf*, 1997]. Breaking results in additional upper ocean turbulence and generation of bubble clouds. Bubbles offer a second pathway for gas transfer between the atmosphere and ocean in addition to direct diffusion across the main interface. Their influence increases with decreasing solubility leading to significant enhancement of the transfer of sparingly soluble gases such as CO_2 under wave breaking conditions relative to calm seas.

The main proxy used to quantify breaking processes is the whitecap fraction (W) which is detectable in near surface imagery from ships or aircrafts (e.g., *Brumer et al.* [2017] and references therein) and can be retrieved from satellite data [*Anguelova and Webster*, 2006]. This has led to parameterizations in which the total [*Zhao et al.*, 2003] or bubble mediated [*Woolf*, 1997; 2005] gas transfer velocities are expressed as a function of W. Similarly to k, W is typically modeled as a non-linear function of wind speed. However, several studies have shown that W can be better constrained by a function of breaking (R_B) and

wave-wind (R_H) Reynolds numbers [*Brumer et al.*, 2017; *Goddijn-Murphy et al.*, 2011; *Zhao and Toba*, 2001]. *Norris et al.* [2013] provided further evidence that wave-breaking related processes may be better constrained by Reynolds numbers than by wind speed alone, showing that the wave-wind Reynolds number is a more adequate predictor for sea-spray aerosol flux than wind speed. These Reynolds numbers incorporate both wave field and wind speed dependence. The wave-wind and breaking Reynolds numbers can be written as: $R_{Hw} = \frac{u_* H_S}{\nu_w}$, and $R_{Bw} = \frac{u_*^2}{\nu_w \omega_p}$, respectively, where u_* is the friction velocity, H_s is the significant wave height, ν_w is the viscosity of water, and ω_p is the peak angular frequency of the wave energy spectrum. The use of the water viscosity is denoted by the "*w*" subscript.

Zhao et al. [2003] combined a parameterization that expresses k_{CO_2} as a power law of *W* based on data from *Wanninkhof et al.* [1995] and the relation of *W* and R_B from *Zhao and Toba* [2001]. They deduced:

$$k_{660} = 0.13\, R_{Ba}^{0.63}, \qquad (2)$$

where k_{660} is the gas velocity normalized to a Schmidt number, *Sc*, of 660 in units of cm h^{-1}. Note that they used the air viscosity (ν_a) rather than the water viscosity for their Reynolds number calculations, hence the "*a*" subscript. Using wind tunnel data from *Jähne et al.* [1985], they further suggested:

$$k_{660} = 0.25\, R_{Ba}^{0.67}. \qquad (3)$$

Woolf [2005] built on his earlier model [*Woolf*, 1997] which separates breaking (k_b), whitecap-dependent, from non-breaking (k_0, u_*, and *Sc*-dependent) contributions and expressed the CO_2 gas transfer velocity as:

$$k = k_0 + k_b = 1.57 \times 10^{-4} u_* \left(\frac{600}{Sc}\right)^{1/2} + 2 \times 10^{-5} R_{Hw}. \qquad (4)$$

Note, this model does not explicitly account for the solubility dependence of k_b, but is consistent with measurements of CO_2 transfer at 20ºC. Equation 4 may therefore only be used for low solubility gases such as CO_2 and requires modification to be applicable to other gases (see *Jeffery et al.* [2010]).

Note that these relationships were determined for growing wind sea conditions. Recent studies [*Brumer et al.*, 2017; *Goddijn-Murphy et al.*, 2011] showed that statistics computed from the total wave spectra, including swells, captured observed variability in *W* as well as wind-sea only statistics suggesting an extended applicability of Reynolds number parameterizations. To date few gas transfer measurements have been made with concurrent wave physics observations and the universality of these parameterizations has yet to be assessed. In this paper, data from four field projects will be used to evaluate Reynolds number parameterizations for CO_2 and DMS and their performance is contrasted to that of wind-only relationships.

2. Data and Methods

Direct eddy covariance measurements of CO_2 were obtained in the North Atlantic during wind speeds up to ~15 m s^{-1} during GasEx-98 [*McGillis et al.*, 2001]. No wave measurements were made during GasEx-98. Instead, wave field statistics were computed from a WAVEWATCHIII® (WW3) global hindcast obtained from the database of the French Research Institute for Exploitation of the Sea (IFREMER) where 3-hourly statistics derived from the total spectrum with a 0.5º spatial resolution are archived (ftp://ftp.ifremer.fr/ifremer/ww3/HINDCAST/GLOBAL/1998_CFSR/).

The Southern Ocean (SO) GasEx cruise, which took place in the South Atlantic, made available eddy covariance measurements of CO_2 and DMS during wind speeds averaging 9.7±3.2 m s^{-1} with a maximum of ~18 m s^{-1} [*Edson et al.*, 2011; *Ho et al.*, 2011; *Yang et al.*, 2011]. A Riegl laser altimeter (model LD90-3100VHS) and a Wave and Surface Current Monitoring System (WAMOS® II) provided wave field data [*Cifuentes-Lorenzen et al.*, 2013; *Lund et al.*, 2017]. The WAMOS resolves the directional wave, whereas the Riegl provides only onmidirectional information. Wave field statistics are consistent between the Riegl and WAMOS, but WAMOS allows separation of wind-sea and swell components. As the WAMOS was not running during the large storm that occurred during the SO GasEx 5-day return transit, the wave data were supplemented by a WW3 global hindcast from the IFREMER database

(ftp://ftp.ifremer.fr/ifremer/ww3/HINDCAST/GLOBAL/2008_ECMWF/). *Lund et al.* [2017] found excellent agreement between the WAMOS and this hindcast for SO GasEX.

Eddy covariance measurements of air–sea CO_2 and DMS fluxes were also made during the Knorr11 cruise, which took place in the North Atlantic Ocean, during wind speeds ranging from ~2 to 20 m s^{-1} [*Bell et al.*, 2013; *Bell et al.*, 2017]. Omnidirectional surface wave spectra were obtained using an ultrasonic altimeter [*Christensen et al.*, 2013]. The significant wave heights measured during Knorr11 agree well with re-analysis and satellite data regardless of whether the ship was on station or not. Good agreement was found between the measured and modeled peak frequencies only while on station. Underway estimates of ω_p are therefore discarded.

The latest direct eddy correlation fluxes of CO_2 and DMS were made during the High Wind Gas exchange Study (HiWinGS) [*Blomquist et al.*, 2017; *Brumer et al.*, 2017; *Yang et al.*, 2014] at wind speeds up to ~25 m s^{-1}. The wave field was monitored with a Riegl laser altimeter and a Datawell DWR-4G Waverider buoy. Buoy wave measurements were only acquired on-station (approximately 68% of the cruise duration). They were supplemented by a cruise specific WW3 hindcast for the entire period of the cruise. The WW3 hindcast, described in *Brumer et al.* [2017], matches the buoy measurements well and provide the most complete dataset. The model directional spectra along the cruise track will be used for the results reported here.

Computation of wave-field statistics

Hourly data are used from all experiments except Knorr11, for which two-hourly timeseries were provided. Wave field statistics were computed from the directional wave spectra obtained from the WAMOS and WW3 hindcasts. The 3-hourly global hindcast fields of *Hs* and *fp* derived from the total

spectrum were interpolated first in space onto the ship's track and then in time to match gas transfer velocity estimates. Separation of the wind-sea and swell systems was achieved based on *Hanson and Phillips* [2001]. While hourly gas transfer velocities were computed for SO GasEx, WAMOS spectra and statistics were computed over 10.25 minutes and averaged to match the gas transfer velocity time resolution. For HiWinGS, the hindcast statistics were obtained half hourly for each of 4 grid points around the ship position and averaged to give a single hourly time series matching the gas fluxes. The significant wave height is defined as follows: $H_s = 4[\int E(f)df]^{1/2}$, where $E(f)$ is either the total omnidirectional wave spectrum or the wind-sea partition. The peak angular velocity is determined from the peak frequency of each system of the whole spectrum: $\omega_p = 2\pi f_p$. In what follows, statistics computed from the wind-sea partition are denoted by a "*ws*" subscript.

Determination and evaluation of gas transfer velocity parameterizations

The gas transfer velocities of CO_2 ($k_{CO_{2660}}$) and DMS ($k_{DMS_{660}}$) were referenced to a Schmidt number of 660 which corresponds to that of CO_2 at 20ºC. For each experiment and gas, seven different parameterizations are considered. Quadratic ($k = aU_{10N}^2+b$), cubic ($k = aU_{10N}^3+b$), and power-law ($k = aU_{10N}^n$) dependence on wind speed were evaluated as well as power-law dependence ($k = aRe^n$) on the wave-wind and breaking Reynolds numbers computed from the total wave spectra and wind-sea partition only. Note, for GasEx-98, Knorr11, and the return transit leg of SO GasEx no wind-sea statistics could be determined. Also, no DMS measurements were taken during GasEx-98. Combining all data, a final set of parameterization is suggested.

Coefficients (*a*, *b* and *n*) were determined through weighted least-square regressions using equi-density bins containing 15 data points. The weights were set to equal the reciprocal of the variance in each bin. Wind-sea statistics for $k_{CO_{2660}}$ were determined from bins of 5 data points due to the paucity of data

178 available from the SO GasEx experiment. In order to compare the performance of the different
179 parameterizations, three metrics are considered: 1) the variation of the exponent "*n*" among the four
180 datasets, 2) the correlation coefficient (r^2), and 3) the root mean square error (*rmse*). Both the r^2 and *rmse*
181 were computed with respect to the hourly and two-hourly data.

182 **3. Results**

183 Key results and parameterizations determined from the four individual and the combined datasets are
184 summarized below. Coefficients for various best-fit functions are reported in Tables 1 and 2 for CO_2 and
185 DMS, respectively.

186

187 $\underline{CO_2}$

188 Figure 1a shows the measured gas transfer velocities of CO_2 plotted against the neutral 10-m wind speed.
189 The different dependences of the $k_{CO_{2660}}$ on U_{10N} observed during the 4 experiments are immediately
190 apparent. While both GasEx datasets show close to cubic wind speed dependence with power-law fit
191 exponents of 2.53 and 2.67 for GasEx-98and SO GasEx, respectively, an exponent of 1.62 best fits the
192 HiWinGS data. The Knorr11 dataset displays the weakest wind speed dependence with a power-law
193 exponent of 1.46. The near-cubic dependences of $k_{CO_{2660}}$ with U_{10N} are in agreement with those reported
194 in *Edson et al.* [2011] and *McGillis et al.* [2001] for the two GasEx datasets. Quadratic parameterizations
195 reported in *Wanninkhof* [1992] or *Ho et al.* [2006] under-predict all but the Knorr11 $k_{CO_{2660}}$.

196

197 The wave-wind Reynolds number, computed from the total wave spectrum (Figure 2a), collapses the
198 observations from all four experiments to a single curve with reduced scatter:

199 $$k_{CO_{2660}} = 2.04 \times 10^{-4} R_{Hw}^{0.88} \qquad (5)$$

200 with r^2 = 0.65 and *rmse* = 29.4 for all datasets combined. These fit statistics are slightly better than those
201 obtained from wind-only fits (Table 1, Eq. p25). Equation 5 captures 58%, 31%, 63%, and 69% of the
202 observed variability in the GasEx-98 (*rmse* = 16.4), SO GasEx (*rmse* = 59.2), Knorr11 (*rmse* = 13.9), and
203 HiWinGS (*rmse* = 27.8) measurements, respectively. A wind speed only power-law parameterization
204 based on the combined dataset captures 60%, 25%, 70%, and 64% of the observed variability in the
205 GasEx-98 (*rmse* = 16.3), SO GasEx (*rmse* = 61.6), Knorr11 (*rmse* = 16), and HiWinGS (*rmse* = 30.1)
206 measurements, respectively.

207

208 Note that not only were more measurements taken during HiWinGS than during the other experiments,
209 but they were also spread over a wider range of wave and wind conditions. These combined fits are
210 therefore mostly driven by the HiWinGS data. Nevertheless, fits to individual data sets also demonstrate
211 improved inter-dataset agreement with wave-wind Reynolds number compared to wind only. Power-law
212 exponents of these fits, ranging from 0.66 (Knorr11) to 1.11 (GasEx-98), show less spread than those of
213 wind speed power laws. Again, project specific wave-wind Reynolds number fits suggest marginal
214 improvement compared to the best individual wind-only fits in terms of r^2 for HiWinGS and SO GasEx.

215

216 The breaking Reynolds number (Figure 2c), collapses the datasets, with power law exponents ranging
217 from 0.52 (Knorr11) to 0.79 (GasEx-98). However, scatter is increased in comparison to the wind-wave
218 Reynolds number for all experiments but GasEx-98. The best fit obtained from the combination of the
219 datasets is:

220 $$k_{CO_2660} = 9.05 \times 10^{-3} R_{Bw}^{0.69} \qquad (6)$$

221 with r^2 = 0.59 and *rmse* = 31.7 for all datasets combined. Equation 6 captures 32%, 27%, 89%, and 65%
222 of the observed variability in the GasEx-98 (*rmse* = 22), SO GasEx (*rmse* = 60.5), Knorr11 (*rmse* = 19.2),
223 and HiWinGS (*rmse* = 29.3) measurements, respectively. As for the wave-wind Reynolds number, the

close match between the combined and dataset specific fit statistics attest to the inter data set agreement of these Reynolds number parameterizations.

Utilizing only the wind-sea part of the spectrum to compute the significant wave height and peak angular frequencies does not lead to improved inter-dataset agreement based on project specific fits (Figure 2b, d). Compared to full sea state Reynolds numbers, the scatter is increased for $R_{Hw_{ws}}$ for which the best fit (Table 1, Eq. p28) only captures 47% of the variability and there is improvement for $R_{Bw_{ws}}$ which captures 53% (Table 1, Eq. p29) of the variability of the So GasEx and HiWinGS data combined. Very few good measurements of $k_{CO_{2660}}$ were taken during SO GasEx with wind sea present.Therefore, best fits determined from both datasets are again mainly driven by the HiWinGS dataset.Project specific fits for SO GasEX have $r^2 \leq 0.05$. Note that for HiWinGS, fits and statistics for $R_{Bw_{ws}}$ are very similar to those for R_{Bw}.

DMS

$k_{DMS_{660}}$ measured during SO GasEx was significantly lower than that measured during HiWinGS for a given wind speed (Figure 1b). The Knorr11 measurements agree with those from HiWinGS for U_{10N} <10 m s^{-1}, however for U_{10N} >14 m s^{-1} they match the lower SO GasEx values. The data recorded when U_{10N} exceeded 14 m s^{-1} during SO GasEx and Knorr11 appear as outliers in Figure 1b as well as in Figure 3a, c. They correspond to unfilled bin average data points in those figures. The SO GasEx outliers were measured during the return transit leg and the Knorr11 outliers were measured at the last station under high wind and wave height conditions. No directional wave data are available to separate wind-seas from swells for these outliers. They are therefore excluded from Figure 3b, d. Sea state, whitecap, and basic environmental conditions do not explain these outliers. They are excluded from results in Table 2.

247

248 Omitting SO GasEx data taken on the return transit and Knorr11 data for U_{10N} >14 m s $^{-1}$ yields better
249 overall inter-project agreement with a power-law function of wind-speed alone capturing 70% of the
250 variability in the combined data and a *rmse* of 5.8. $k_{DMS_{660}}$ increases close to linearly with wind speed with
251 power-law exponent ranging from 1.28 to 1.4. A power-law function of R_{Hw} captures 57% of the
252 combined variability with *rmse* = 6.8:

253 $$k_{DMS_{660}} = 1.95 \times 10^{-2} R_{Hw}^{0.49}. \quad (7)$$

254 A power-law function of R_{Bw} can account for 63% of the variability in both data sets with *rmse* of 6.4:

255 $$k_{DMS_{660}} = 5.36 \times 10^{-2} R_{Bw}^{0.47}. \quad (8)$$

256 Considering wind seas only (Table 2, Eqs. p53 and p54) leads to divergence in the individual best fits for
257 the two data sets with comparable statistic to Eqs. 7 and 8. As noted above, the high wind SO GasEx and
258 Knorr11 observations were not included in these fits.

259

260 When considering the datasets individually, expressing $k_{DMS_{660}}$ as a function of Reynolds numbers does
261 not lead to better fit statistics than wind only fits. Indeed, for SO GasEX a wind speed power-law
262 dependence can capture 45% of the variability while a breaking Reynolds number dependence only
263 captures 25% when ignoring the above mentioned outliers. For Knorr11, the wind speed and R_{Bw} perform
264 comparably well, allowing accounting for 38% and 39% of the observed variability for U_{10N} <14 m s^{-1}.
265 For HiWinGS, the wind speed only parameterization performs only slightly better than the R_{Bw} one with
266 75% compared to 71%. Power law exponents for the fits to the individual datasets are comparably close
267 for wind-speed and both Reynolds numbers. It is possible that the potential improvement in fit statistics
268 using Reynolds number instead of wind speed is offset by the greater sampling error in determining wave
269 statistics.

4. Discussion

Wind-only *k* parameterizations display significant disagreement between different studies [*Garbe et al.*, 2014; *Goddijn-Murphy et al.*, 2012; *McGillis et al.*, 2001; *Wanninkhof*, 1992]. While implementing different wind-only parameterizations for CO_2 may result in comparable globally averaged gas transfer velocities, the parameterization choice was shown to have significant impact on regional fluxes [*Fangohr and Woolf*, 2007; *Wrobel and Piskozub*, 2016]. In light of current efforts to include wave processes in Earth System models (e.g., *Li et al.* [2016]; *Qiao et al.* [2013]), it is time to update the traditional wind-only gas transfer parameterizations to sea state dependent ones and assess uncertainties linked to the choice of parameterization.

Parameterizations that incorporate the dependence of wind and sea state in the form of a wave-wind and breaking Reynolds number provide coherent agreement between the GasEx-98, SO GasEx, Knorr11, and HiWinGS datasets for CO_2, and the majority of the DMS data. This study therefore strongly suggests that expressing *k* as a simple function of a wave-related Reynolds number will lead to improved parameterizations for regional and global models relative to wind-only parameterizations. Global fields of significant wave heights and peak angular velocities are routinely computed by operational wave prediction centers, making wave-wind and breaking Reynolds number based parameterizations convenient to implement and test on a global scale. The relationships between *k* and other wave statistics such as the wave age, bulk slope, and the mean square steepness were also examined but did not reveal significant trends or yield reduced scatter between projects.

Although the current study is not a comprehensive analysis of all available eddy covariance CO_2 and DMS gas transfer data, the datasets analyzed here are representative of the observed variability. They

were chosen because they span a wide range of wind speeds with strongly differing dependencies. They are also, to the best of our knowledge, the only available gas transfer datasets with in situ wave field measurements. Wave model hindcasts could extend this analysis to other existing CO_2 and DMS datasets [*Bell et al.*, 2015; *Blomquist et al.*, 2006; *Huebert et al.*, 2004; *Marandino et al.*, 2007; 2008; 2009; *Miller et al.*, 2009]. However, these datasets span a more limited and lower range of wind speeds and may not add much additional information because discrepancies in k at low wind speeds are small.

CO_2 and DMS have solubilities of ~1 and ~20, which strongly influence the fraction of total transfer resistance represented by bubble-mediated and air-side mechanisms. The less soluble a gas, the more its air-sea flux depends on the transfer resistance in the aqueous boundary layer and bubble mediated mechanisms. This explains why k_{DMS} is smaller than k_{CO_2} at high wind speeds, where wave breaking leads to generation of bubble clouds, and thus the need for different, single parameter models for gases of different solubilities. One could a priori expect DMS to be less sea state dependent than CO_2 as its increased solubility means that its transfer velocity depends less on bubble mediated transfer. Weaker dependence on sea state may account for the increased scatter observed in the relationship between both the wave-wind and breaking Reynolds numbers and $k_{DMS_{660}}$. Sea state, represented as either the significant wave height or wave age ($\beta = g/(\omega_p u_*) = R_{Bw}(g\nu_w)/u_*^3$) does not reconcile outliers in the SO GasEx and Knorr11 DMS dataset. These suppressed gas transfer velocities at high wind speeds were observed in high wave height conditions, i.e. high R_{Hw} and more work is needed to understand these observations. *Bell et al.* [2013] suggest that young, large waves may influence interfacial gas transfer by either causing airflow separation at the wave crest or by modulating the microbreaking of small-scale waves.

Early studies [*Toba and Koga*, 1986; *Zhao and Toba*, 2001; *Zhao et al.*, 2003] which relate breaking conditions, whitecapping, and gas transfer velocities to Reynolds numbers focus on wind-sea statistics, ignoring the importance of swell. It is typically assumed that wave breaking is governed by the wind sea component of the wave spectrum, and that properties of the wind sea partition are most relevant for air-sea processes. This study, however, suggests that consideration of swell is important for gas transfer. Indeed, considering only the wind-sea partition of the wave spectra did not reduce the scatter in k, yielding poor fits that differ substantially between datasets. Arguably this could be due to the paucity of data collected under wind-sea conditions especially during SO GasEx or the difficulty of separating wind-sea and swell. More data are needed to verify this. However, non-breaking wave induced mixing has been shown to significantly contribute to upper ocean turbulence through Langmuir circulation [*Fan and Griffies*, 2014; *Li et al.*, 2016]. This suggests mixing that arises from all components of the wave spectra should be considered. Furthermore, if large waves indeed inhibit interfacial gas transfer, the swell component needs to be considered. Reynolds numbers computed from the full spectrum can, however, not account for this effect.

The Reynolds number parameterizations determined in this study differ from previously published parameterizations [*Woolf*, 2005; *Zhao et al.*, 2003] using the wind-sea partition or the total spectra. This can partially be attributed to the whitecap data used to tune previous parameterizations. The W parameterization used by *Zhao and Toba* [2001] overestimates W measured during both experiments resulting in overestimated gas transfer velocities. The parameterization of *Woolf* [2005] underestimates the measured transfer velocities of CO_2 though it is loosely based on the relation between W and R_{Ha} determined by *Zhao and Toba* [2001]. The issue here comes primarily from the relation used between the bubble mediated transfer and W based on *Woolf* [1997], but may also be attributed to the expression for non-breaking transfer used. The coefficients of the 1997 bubble mediated transfer model are best guess values which were tuned in *Woolf* [2005] to match a range of observed functions given the assumption

342 that wave fetch is the primary controlling parameter for *W*. The model may therefore not be adequate for
343 the open ocean. Note also that we established that these earlier *W* data and the parameterizations differ
344 greatly from recent observations [*Brumer et al.*, 2017] in part due to the different techniques employed,
345 and in part due to different wind/wave environments (pure wind vs. mixed seas, laboratory or fetch
346 limited vs. open ocean waves).

347

348 **5. Conclusion**

349 Breaking and wind wave Reynolds numbers allow for improved single parameter models of the gas
350 transfer velocity of DMS and CO_2 relative to wind speed only parameterizations. The Reynolds number-
351 based parameterizations appear to be more universally valid, collapsing the data of the GasEx-98, SO
352 GasEx, Knorr11, and HiWinGS experiments onto closely matching power law dependences, while wind
353 only parameterizations vary greatly between datasets. For CO_2 they also, for the most part, capture
354 slightly more of the observed variability than the traditional wind only ones. The comparable goodness of
355 fits for wind speed and wave related Reynolds numbers reflects the natural high variability of individual
356 flux estimates which does not vary much for a single set of wind/wave conditions. The important result is
357 that the wave related Reynolds numbers provide a dramatic improvement in reconciling *k* results from
358 very different wind/wave regimes. Unlike previous studies that relied on the combination of unrelated
359 datasets and approximate relations between Reynolds numbers, whitecap fraction and gas transfer
360 velocities, here we show the first Reynolds number parameterizations determined directly from
361 concurrent eddy covariance measurements of gas fluxes and modeled or remotely sensed wave field
362 statistics.

363

6. Acknowledgments

This work was funded by the National Science Foundation (Grants OCE-0647667, OCE-0647475, OCE-1537890, AGS-1036062, AGS-1036006, AGS-1444294), the National Oceanic and Atmospheric Administration (Grant NA07OAR4310094, NA07OAR4310084), and the Natural Environment Research Council (grant NE/J020893/1). Data from the HiWinGS cruise will be made publicly available on the NOAA FTP server: ftp://ftp1.esrl.noaa.gov/psd3/cruises/HIWINGS_2013/Collective_Archive. The SO GasEX data can be found on: http://www.bco-dmo.org/project/2064. The authors would like to thank D.K. Woolf and T.G. Bell for reviewing this manuscript. T.G. Bell kindly provided the Knorr11 data used here. This is Lamont-Doherty Earth Observatory contribution number 8146.

7. References

Anguelova, M. D., and F. Webster (2006), Whitecap coverage from satellite measurements: A first step toward modeling the variability of oceanic whitecaps, J. Geophys. Res., 111(C03017), doi:10.1029/2005JC003158.

Arora, V. K., G. J. Boer, P. Friedlingstein, M. Eby, C. D. Jones, J. R. Christian, G. Bonan, L. Bopp, V. Brovkin, P. Cadule, T. Hajima, T. Ilyina, K. Lindsay, J. F. Tjiputra, and T. Wu (2013), Carbon–Concentration and Carbon–Climate Feedbacks in CMIP5 Earth System Models, Journal of Climate, 26(15), 5289-5314, doi: 10.1175/jcli-d-12-00494.1.

Bell, T. G., W. De Bruyn, S. Miller, B. Ward, K. Christensen, and E. Saltzman (2013), Air–sea dimethylsulfide (DMS) gas transfer in the North Atlantic: evidence for limited interfacial gas exchange at high wind speed, Atmospheric Chemistry and Physics, 13(21), 11073-11087.

Bell, T. G., W. De Bruyn, C. A. Marandino, S. D. Miller, C. S. Law, M. J. Smith, and E. S. Saltzman (2015), Dimethylsulfide gas transfer coefficients from algal blooms in the Southern Ocean, Atmos. Chem. Phys., 15(4), 1783-1794, doi: 10.5194/acp-15-1783-2015.

Bell, T. G., S. Landwehr, S. D. Miller, W. J. de Bruyn, A. Callaghan, B. Scanlon, B. Ward, M. Yang, and E. S. Saltzman (2017), Estimation of bubbled-mediated air/sea gas exchange from concurrent DMS and CO2 transfer velocities at intermediate-high wind speeds, Atmos. Chem. Phys. Discuss., 2017, 1-29, doi: 10.5194/acp-2017-85.

Blomquist, B. W., C. W. Fairall, B. J. Huebert, D. J. Kieber, and G. R. Westby (2006), DMS sea-air transfer velocity: Direct measurements by eddy covariance and parameterization based on the NOAA/COARE gas transfer model, Geophysical Research Letters, 33(7), Art. No. L07601.

Blomquist, B. W., S. E. Brumer, C. W. Fairall, B. J. Huebert, C. J. Zappa, I. M. Brooks, M. Yang, L. Bariteau, J. Prytherch, J. E. Hare, H. Czerski, A. Matei, and R. W. Pascal (2017), Wind speed and sea state dependencies of air-sea gas transfer: results from the High Wind speed Gas exchange Study (HiWinGS), Journal of Geophysical Research - Oceans, doi: 10.002/2017JC013181.

401 Brumer, S. E., C. J. Zappa, I. M. Brooks, H. Tamura, S. M. Brown, B. Blomquist, C. W. Fairall,
402 and A. Cifuentes-Lorenzen (2017), Whitecap coverage dependence on wind and wave
403 statistics as observed during SO GasEx and HiWinGS, Journal of Physical Oceanography,
404 doi: DOI: 10.1175/JPO-D-17-0005.1.
405 Carpenter, L. J., S. D. Archer, and R. Beale (2012), Ocean-atmosphere trace gas exchange,
406 Chemical Society Reviews, 41(19), 6473-6506, doi: 10.1039/c2cs35121h.
407 Charlson, R. J., J. E. Lovelock, M. O. Andreae, and S. G. Warren (1987), Oceanic phytoplankton,
408 atmospheric sulphur, cloud albedo and climate, Nature, 326, 655-660.
409 Christensen, K. H., J. Röhrs, B. Ward, I. Fer, G. Broström, Ø. Saetra, and Ø. Breivik (2013),
410 Surface wave measurements using a ship-mounted ultrasonic altimeter, Methods in
411 Oceanography, 6(0), 1-15, doi: http://dx.doi.org/10.1016/j.mio.2013.07.002.
412 Cifuentes-Lorenzen, A., J. B. Edson, C. J. Zappa, and L. Bariteau (2013), A multi-sensor
413 comparison of ocean wave frequency spectra from a research vessel during the Southern
414 Ocean Gas Exchange Experiment, J. Atmos. Oceanic Tech., 30(12), 2907-2925, doi:
415 10.1175/JTECH-D-12-00181.1.
416 Edson, J. B., C. W. Fairall, L. Bariteau, C. J. Zappa, A. Cifuentes-Lorenzen, W. R. McGillis, S.
417 Pezoa, J. E. Hare, and D. Helmig (2011), Direct covariance measurement of CO_2 gas
418 transfer velocity during the 2008 Southern Ocean Gas Exchange Experiment: Wind speed
419 dependency, Journal of Geophysical Research – Oceans, 116(C4), C00F10, doi:
420 10.1029/2011JC007022.
421 Fan, Y., and S. M. Griffies (2014), Impacts of Parameterized Langmuir Turbulence and
422 Nonbreaking Wave Mixing in Global Climate Simulations, Journal of Climate, 27(12),
423 4752-4775, doi: 10.1175/jcli-d-13-00583.1.
424 Fangohr, S., and D. K. Woolf (2007), Application of new parameterizations of gas transfer velocity
425 and their impact on regional and global marine CO2 budgets, Journal of Marine Systems,
426 66(1–4), 195-203, doi: http://dx.doi.org/10.1016/j.jmarsys.2006.01.012.
427 Garbe, C. S., A. Rutgersson, J. Boutin, G. d. Leeuw, B. Delille, C. W. Fairall, N. Gruber, J. Hare,
428 D. T. Ho, M. T. Johnson, P. D. Nightingale, H. Pettersson, E. S. Jacek Piskozub, W.-t. Tsai,
429 B. Ward, D. K. Woolf, and C. J. Zappa (2014), Transfer across the air-sea interface, in
430 Ocean-Atmosphere Interactions of Gases and Particles, edited by P. S. Liss and M. T.
431 Johnson, pp. 55-112, Springer Berlin Heidelberg.
432 Goddijn-Murphy, L., D. K. Woolf, and A. H. Callaghan (2011), Parameterizations and algorithms
433 for oceanic whitecap coverage, Journal of Physical Oceanography, 41(4), 742-756.
434 Goddijn-Murphy, L., D. K. Woolf, and C. Marandino (2012), Space-based retrievals of air-sea gas
435 transfer velocities using altimeters: Calibration for dimethyl sulfide, Journal of
436 Geophysical Research: Oceans, 117(C8), C08028, doi: 10.1029/2011JC007535.
437 Hanson, J. L., and O. M. Phillips (2001), Automated Analysis of Ocean Surface Directional Wave
438 Spectra, Journal of Atmospheric and Oceanic Technology, 18(2), 277-293, doi:
439 10.1175/1520-0426(2001)018<0277:AAOOSD>2.0.CO;2.
440 Ho, D. T., C. S. Law, M. J. Smith, P. Schlosser, M. Harvey, and P. Hill (2006), Measurements of
441 air-sea gas exchange at high wind speeds in the Southern Ocean: Implications for global
442 parameterizations, Geophys. Res. Lett., 33, L16611, doi: 10.1029/2006GL026817.
443 Ho, D. T., R. Wanninkhof, P. Schlosser, D. S. Ullman, D. Hebert, and K. F. Sullivan (2011),
444 Toward a universal relationship between wind speed and gas exchange: Gas transfer
445 velocities measured with 3He/SF6 during the Southern Ocean Gas Exchange Experiment,
446 Journal of Geophysical Research: Oceans, 116(C4), C00f04, doi: 10.1029/2010JC006854.

Huebert, B. J., B. W. Blomquist, J. E. Hare, C. W. Fairall, J. E. Johnson, and T. S. Bates (2004), Measurement of the sea-air DMS flux and transfer velocity using eddy correlation, Geophysical Research Letters, 31, 1--4, doi: 10.1029/2004GL021567.

Jähne, B., K. O. Munnich, R. Bosinger, A. Dutzi, W. Huber, and P. Libner (1987), On the parameters influencing air-water gas exchange, J. Geophys. Res., 92(C2), 1937-1949.

Jähne, B., T. Wais, L. Memery, G. Caulliez, L. Merlivat, K. O. Münnich, and M. Coantic (1985), He and Rn gas exchange experiments in the large wind-wave facility of IMST, J. Geophys. Res., 90(C6), 11989-11997.

Jeffery, C. D., I. S. Robinson, and D. K. Woolf (2010), Tuning a physically-based model of the air–sea gas transfer velocity, Ocean Modelling, 31(1–2), 28-35, doi: http://dx.doi.org/10.1016/j.ocemod.2009.09.001.

Komori, S., R. Nagaosa, and Y. Murakami (1993), Turbulence structure and mass transfer across a sheared air-water interface in wind-driven turbulence, Journal of Fluid Mechanics, 249, 161-183.

Li, Q., A. Webb, B. Fox-Kemper, A. Craig, G. Danabasoglu, W. G. Large, and M. Vertenstein (2016), Langmuir mixing effects on global climate: WAVEWATCH III in CESM, Ocean Modelling, 103, 145-160, doi: http://dx.doi.org/10.1016/j.ocemod.2015.07.020.

Liss, P. S., and L. Merlivat (1986), Air–sea gas exchange rates: Introduction and synthesis, in The Role of Air–Sea Exchange in Geochemical Cycling, edited by P. Buat-Ménard, pp. 113-127, D. Reidel, Dordrecht, Holland.

Lund, B., C. J. Zappa, H. C. Graber, and A. Cifuentes-Lorenzen (2017), Shipboard Wave Measurements in the Southern Ocean, Journal of Atmospheric and Oceanic Technology, 34, 2113-2126, doi: https://doi.org/10.1175/JTECH-D-16-0212.1.

Marandino, C. A., W. J. De Bruyn, S. D. Miller, and E. S. Saltzman (2007), Eddy correlation measurements of the air/sea flux of dimethylsulfide over the North Pacific Ocean, J. Geophys. Res., 112(D3), D03301, doi: 10.1029/2006JD007293.

Marandino, C. A., W. J. De Bruyn, S. D. Miller, and E. S. Saltzman (2008), DMS air/sea flux and gas transfer coefficients from the North Atlantic summertime coccolithophore bloom, Geophysical Research Letters, 35(23), L23812, doi: 10.1029/2008GL036370.

Marandino, C. A., W. J. De Bruyn, S. D. Miller, and E. S. Saltzman (2009), Open ocean DMS air/sea fluxes over the eastern South Pacific Ocean, Atmos. Chem. Phys., 9(2), 345-356, doi: 10.5194/acp-9-345-2009.

McGillis, W. R., J. B. Edson, J. E. Hare, and C. W. Fairall (2001), Direct covariance air-sea CO2 fluxes, J. Geophys. Res., 106(c8), 16729-16745.

Miller, S. D., C. Marandino, W. De Bruyn, and E. S. Saltzman (2009), Air-sea gas exchange of CO2 and DMS in the North Atlantic by eddy covariance, Geophysical Research Letters, 36(15), 1-5, doi: 10.1029/2009GL038907.

Norris, S. J., I. M. Brooks, and D. J. Salisbury (2013), A wave roughness Reynolds number parameterization of the sea spray source flux, Geophysical Research Letters, 40(16), 4415-4419, doi: 10.1002/grl.50795.

Qiao, F., Z. Song, Y. Bao, Y. Song, Q. Shu, C. Huang, and W. Zhao (2013), Development and evaluation of an Earth System Model with surface gravity waves, Journal of Geophysical Research: Oceans, 118(9), 4514-4524, doi: 10.1002/jgrc.20327.

Sweeney, C., E. M. Gloor, A. R. Jacobson, R. M. Key, G. Mckinley, J. L. Sarmiento, and R. Wanninkhof (2007), Constraining global air-sea gas exchange for CO_2 with recent bomb 14C measurements, Glob. Biogeochem. Cycle, 21, GB2015, doi: 10.1029/2006GB002784.

Toba, Y., and M. Koga (1986), A Parameter Describing Overall Conditions of Wave Breaking, Whitecapping, Sea-Spray Production and Wind Stress, in Oceanic Whitecaps, edited by E. Monahan and G. Niocaill, pp. 37-47, Springer Netherlands.

Wanninkhof, R. (1992), Relationship between wind speed and gas exchange over the ocean, J. Geophys. Res., 97(C5), 7373-7382, doi: 10.1029/92JC00188.

Wanninkhof, R. (2014), Relationship between wind speed and gas exchange over the ocean revisited, Limnology and Oceanography: Methods, 12(6), 351-362, doi: 10.4319/lom.2014.12.351.

Wanninkhof, R., and W. R. McGillis (1999a), A cubic relationship between air-sea CO_2 exchange and wind speed, Geophys. Res. Lett., 26(13), 1889-1892.

Wanninkhof, R., and W. R. McGillis (1999b), A cubic relationship between air sea CO2 exchange and wind speed, edited, pp. 1889-1892.

Wanninkhof, R., W. Asher, and E. Monahan (1995), The influence of bubbles on air-water gas exchange: Results from gas transfer experiments during WABEX-93, paper presented at Selected Papers from the Third International Symposium on Air–Water Gas Transfer.

Woolf, D. K. (1997), Bubbles and their role in air–sea gas exchange, in The Sea Surface and Global Change, edited by PS Liss and R. Duce, pp. 173-206, Cambridge Univ Press, Cambridge, UK.

Woolf, D. K. (2005), Parameterization of gas transfer velocities and sea-state-dependent wave breaking, Tellus, 57B, 87-94.

Wrobel, I., and J. Piskozub (2016), Effect of gas-transfer velocity parameterization choice on air–sea CO2 fluxes in the North Atlantic Ocean and the European Arctic, Ocean Sci., 12(5), 1091-1103, doi: 10.5194/os-12-1091-2016.

Yang, M., B. W. Blomquist, and P. D. Nightingale (2014), Air-sea exchange of methanol and acetone during HiWinGS: Estimation of air phase, water phase gas transfer velocities, Journal of Geophysical Research: Oceans, 119(10), 7308-7323, doi: 10.1002/2014JC010227.

Yang, M., B. W. Blomquist, C. W. Fairall, S. D. Archer, and B. J. Huebert (2011), Air-sea exchange of dimethylsulfide in the Southern Ocean: Measurements from SO GasEx compared to temperate and tropical regions, Journal of Geophysical Research: Oceans, 116(C4), C00f05, doi: 10.1029/2010JC006526.

Zhao, D., and Y. Toba (2001), Dependence of whitecap coverage on wind and wind-wave properties, Journal of Oceanography, 57(5), 603-616, doi: 10.1023/A:1021215904955.

Zhao, D., Y. Toba, Y. Suzuki, and S. Komori (2003), Effect of wind waves on air–sea gas exchange: proposal of an overall CO_2 transfer velocity formula as a function of breaking-wave parameter, Tellus, Series B: Chemical and Physical Meteorology, 55B, 478-487, doi: 10.1034/j.1600-0889.2003.00055.x.

List of Figures

Figure 1- Measured gas transfer velocity of a) CO_2 and b) DMS, adjusted to a Schmidt number of 660 and plotted against 10 m neutral wind speed (U_{10N}). The smaller dots represent individual hourly and two-hourly estimates and the larger symbols are averages of equidensity bins of 15 data points. The solid lines represent best fits of power laws of the form $k = ax^n$. Examples of published cubic ($k = aU_{10}^3 + b$) and quadratic ($k = aU_{10}^2 + b$) parameterizations derived from CO_2 datasets are represented by dotted and dashed lines, respectively. Examples of published linear wind-speed dependent parameterization ($k = aU_{10} + b$) derived from DMS measurements are represented by dashed lines in b). The open symbols in b)

List of Tables

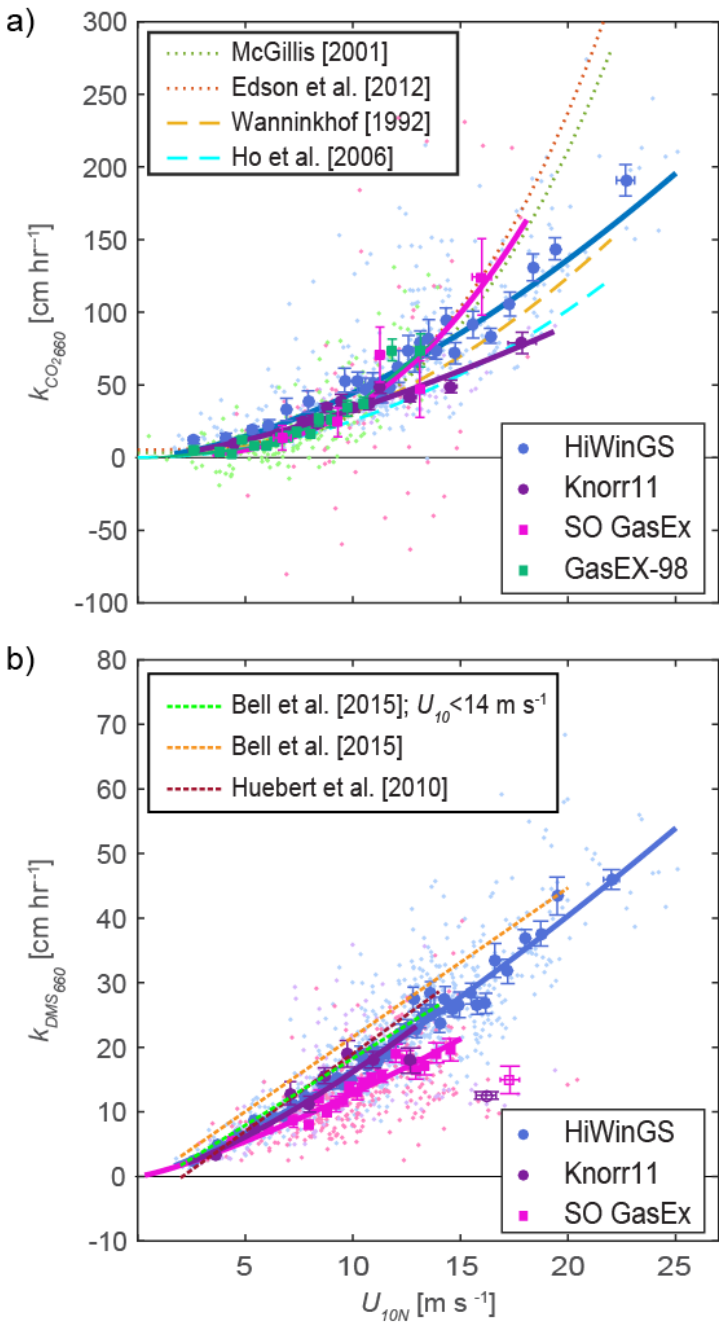

Figure 1- Measured gas transfer velocity of a) CO_2 and b) DMS, adjusted to a Schmidt number of 660 and plotted against 10 m neutral wind speed (U_{10N}). The smaller dots represent individual hourly and two-hourly estimates and the larger symbols are averages of equidensity bins of 15 data points. The solid lines represent best fits of power laws of the form $k = ax^n$. Examples of published cubic ($k = aU_{10}^3 + b$) and quadratic ($k = aU_{10}^2 + b$) parameterizations derived from CO_2 datasets are represented by dotted and dashed lines, respectively. Examples of published linear wind-speed dependent parameterization ($k = aU_{10} + b$) derived from DMS measurements are represented by dashed lines in b). The open symbols in b) represent outliers in the SO GasEx and Knorr11 datasets that cannot be reconciled by either wind speed or Reynolds numbers.

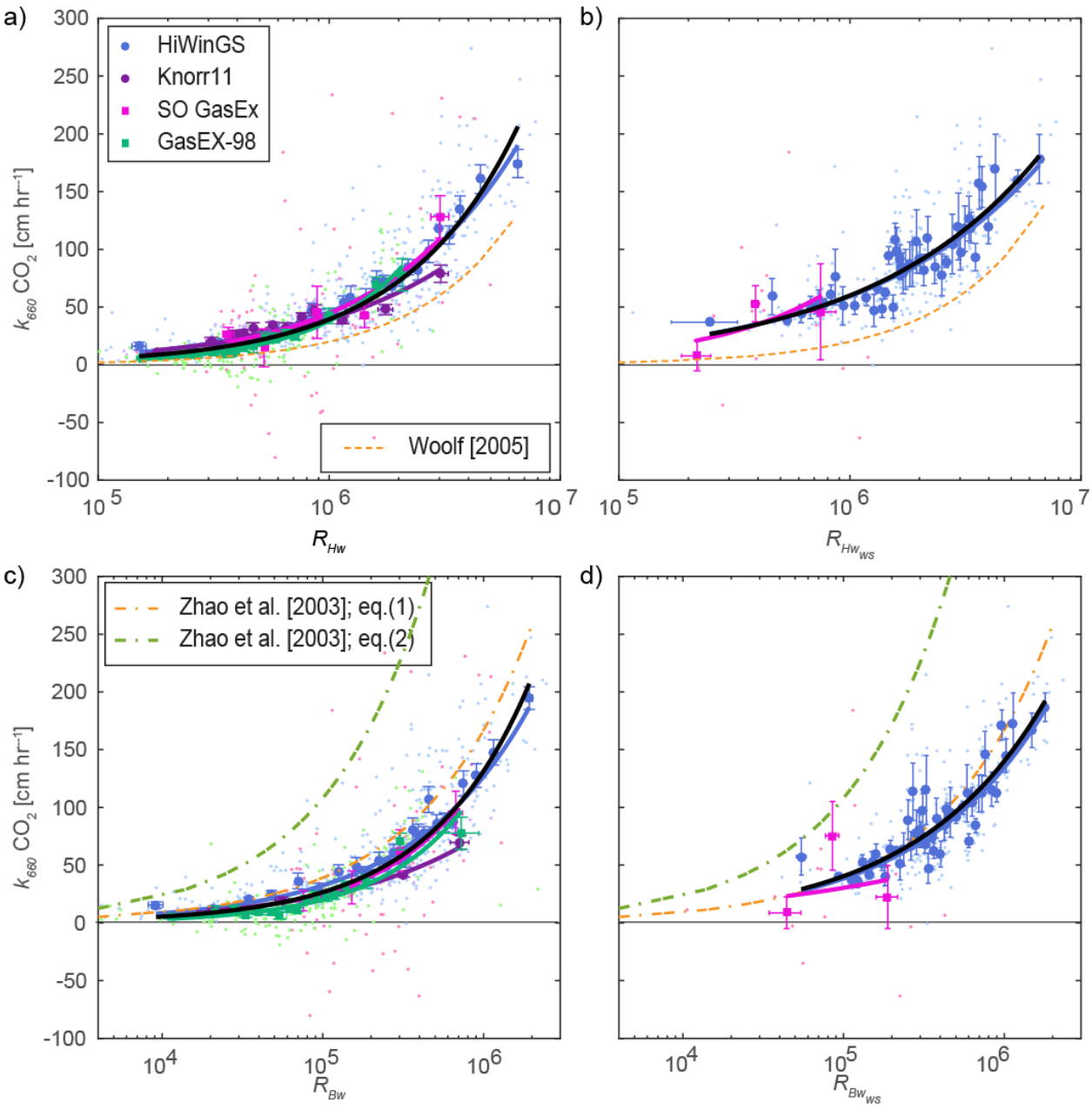

Figure 2- Measured gas transfer velocity of CO_2 adjusted to a Schmidt number of 660 plotted against a) the wave-wind Reynolds number based on H_s computed from the total spectrum, b) the wave-wind Reynolds number based on H_s computed from the wind-sea partition of the wave spectrum, c) the breaking Reynold number computed from the total spectrum, and d) the breaking Reynold number computed from the wind-sea partition of the wave spectrum. The smaller dots represent individual hourly and two hourly estimates, the larger symbols are averages of equidensity bins of 15 data points for a) and c) and 5 points for b) and d). The solid green, pink, and purple, blue, and black lines represent best fits of power laws of the form $k = ax^n$, for Gasex-98, SO GasEx, Knorr11, HiWinGS, and all the data, respectively.

564

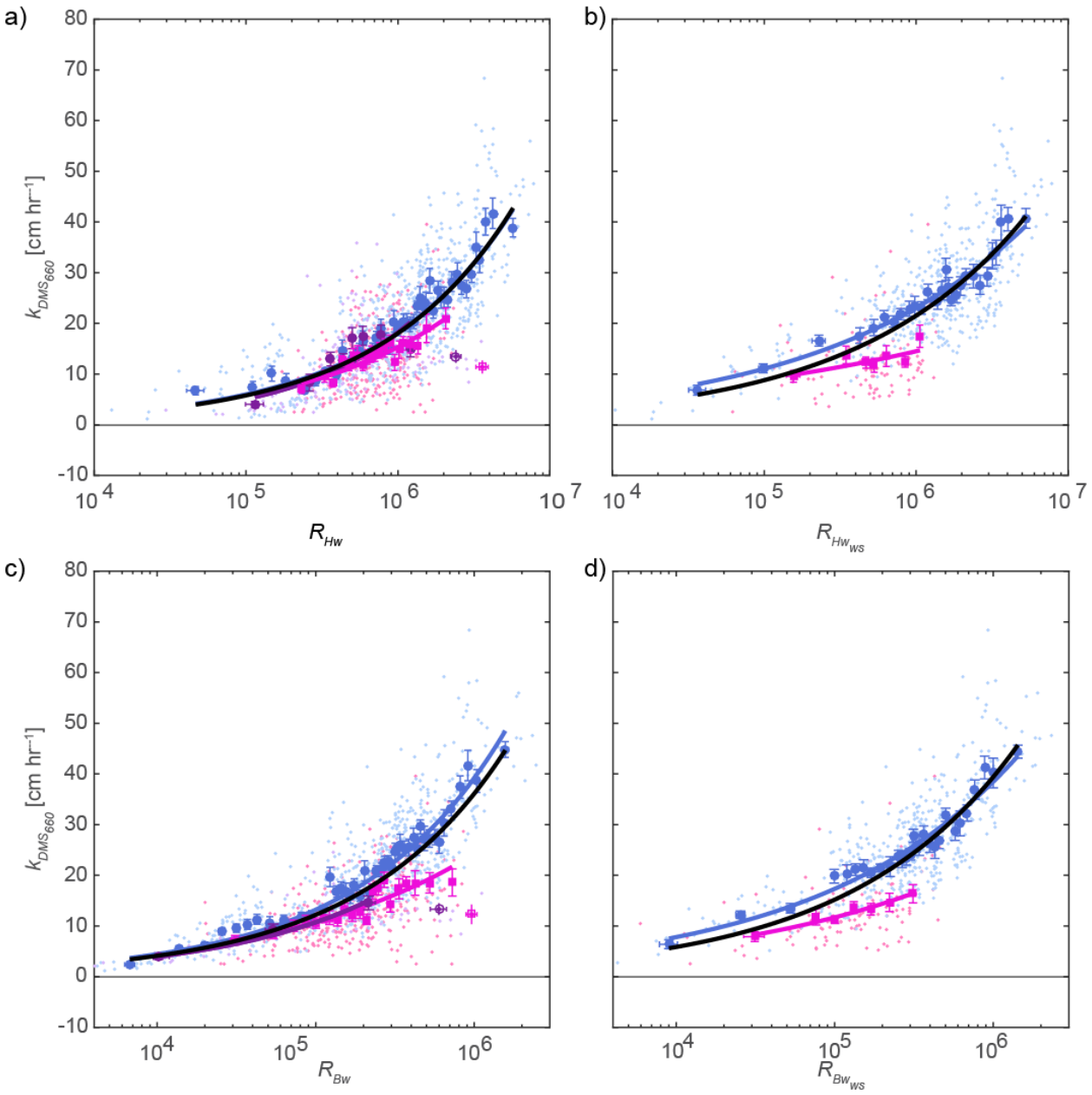

Figure 3- Measured gas transfer velocity of DMS adjusted to a Schmidt number of 660 plotted against a) the wave-wind Reynolds number based on H_s computed from the total spectrum, b) the wave-wind Reynolds number based on H_s computed from the wind-sea partition of the wave spectrum, c) the breaking Reynold number computed from the total spectrum, and d) the breaking Reynold number computed from the wind-sea partition of the wave spectrum. The smaller dots represent individual hourly and two hourly estimates, the larger symbols are averages of equidensity bins of 15 data points. The solid pink, and purple, blue, and black lines represent best fits of power laws of the form $k = ax^n$, for SO GasEx, Knorr11, HiWinGS, and all the data, respectively. The open symbols represent outliers in the SO GasEx and Knorr11 datasets that cannot be reconciled by neither wind speed nor Reynolds numbers.

565 Table 1 – Least square fit results of the wind speed and Reynolds number dependence of the gas transfer

566 velocity of CO_2 referenced to a Schmidt number of 660.

Eq.	Experiment	Form	*a*	*n*	r^2	*rmse*
p1	GasEx-98	$k = a\,(U_{10N})^n$	1.06E-01	2.53	0.62	15.4
p2		$k = a\,(U_{10N})^2 + n$	3.46E-01	-1.30	0.60	16.4
p3		$k = a\,(U_{10N})^3 + n$	3.14E-02	3.48	0.63	15.3
p4		$k = a(R_{Hw})^n$	7.97E-06	1.11	0.57	16.2
p5		$k = a(R_{Bw})^n$	2.27E-03	0.79	0.28	22.4
p6	SO GasEx	$k = a\,(U_{10N})^n$	7.27E-02	2.67	0.25	60.8
p7		$k = a\,(U_{10N})^2 + n$	4.79E-01	-11.01	0.25	60.9
p8		$k = a\,(U_{10N})^3 + n$	2.80E-02	4.78	0.25	60.9
p9		$k = a(R_{Hw})^n$	6.10E-04	0.81	0.31	59.0
p10		$k = a(R_{Bw})^n$	5.75E-03	0.73	0.27	60.45
p11		$k = a(R_{Hw_{ws}})^n$	6.72E-04	0.84	0.05	64.4
p12		$k = a(R_{Bw_{ws}})^n$	7.45E-02	0.51	0.01	58.2
p13	Knorr11	$k = a\,(U_{10N})^n$	1.15E+00	1.46	0.71	9.2
p14		$k = a\,(U_{10N})^2 + n$	2.56E-01	5.78	0.69	10.1
p15		$k = a\,(U_{10N})^3 + n$	1.55E-02	11.45	0.64	12.5
p16		$k = a(R_{Hw})^n$	4.11E-03	0.66	0.64	10.7
p17		$k = a(R_{Bw})^n$	6.33E-02	0.52	0.90	7.2
p18	HiWinGS	$k = a\,(U_{10N})^n$	1.07E+00	1.62	0.63	29.9
p19		$k = a\,(U_{10N})^2 + n$	3.32E-01	9.23	0.64	29.7
p20		$k = a\,(U_{10N})^3 + n$	1.74E-02	18.47	0.61	31.9
p21		$k = a(R_{Hw})^n$	1.25E-03	0.76	0.69	27.1
p22		$k = a(R_{Bw})^n$	3.63E-02	0.59	0.66	28.7
p23		$k = a(R_{Hw_{ws}})^n$	2.33E-02	0.57	0.48	34.7
p24		$k = a(R_{Bw_{ws}})^n$	7.73E-02	0.54	0.55	33.0
p25	Combined	$k = a\,(U_{10N})^n$	4.78E-01	1.91	0.61	29.8
p26		$k = a(R_{Hw})^n$	2.04E-04	0.88	0.65	29.4
p27		$k = a(R_{Bw})^n$	9.05E-03	0.69	0.59	31.7
p28		$k = a(R_{Hw_{ws}})^n$	1.64E-02	0.59	0.47	36.7
p29		$k = a(R_{Bw_{ws}})^n$	5.70E-02	0.56	0.53	35.0

567

568

569 *Table 2– Least square fit results of the wind speed and Reynold number dependence of the gas transfer*

570 *velocity of DMS referenced to a Schmidt number of 660.*

Eq.	Experiment	Form	*a*	*n*	r^2	*rmse*
p30	SO GasEx	$k = a\,(U_{10N})^n$	7.31E-01	1.25	0.25	5.8
p31		$k = a\,(U_{10N})^2 + n$	8.51E-02	3.95	0.20	6.4
p32		$k = a\,(U_{10N})^3 + n$	5.69E-03	6.20	0.13	7.8
p33		$k = a(R_{Hw})^n$	3.75E-02	0.44	0.18	5.9
p34		$k = a(R_{Bw})^n$	1.91E-01	0.35	0.25	5.6
p35		$k = a(R_{Hw_{ws}})^n$	8.22E-01	0.21	0.08	6.1
p36		$k = a(R_{Bw_{ws}})^n$	3.72E-01	0.30	0.22	5.6
p37	Knorr11	$k = a\,(U_{10N})^n$	6.45E-01	1.40	0.38	6.0
p38		$k = a\,(U_{10N})^2 + n$	1.40E-01	2.11	0.34	6.5
p39		$k = a\,(U_{10N})^3 + n$	1.11E-02	3.78	0.26	7.3
p40		$k = a(R_{Hw})^n$	7.62E-03	0.56	0.20	6.8
p41		$k = a(R_{Bw})^n$	7.14E-02	0.44	0.39	6.3
p42	HiWinGS	$k = a\,(U_{10N})^n$	8.23E-01	1.30	0.75	5.7
p43		$k = a\,(U_{10N})^2 + n$	1.07E-01	3.78	0.73	6.2
p44		$k = a\,(U_{10N})^3 + n$	5.53E-03	6.40	0.65	8.0
p45		$k = a(R_{Hw})^n$	2.28E-02	0.48	0.62	7.0
p46		$k = a(R_{Bw})^n$	5.73E-02	0.47	0.71	6.0
p47		$k = a(R_{Hw_{ws}})^n$	2.80E-01	0.32	0.54	7.0
p48		$k = a(R_{Bw_{ws}})^n$	3.22E-01	0.35	0.63	6.3
p50	Combined	$k = a\,(U_{10N})^n$	7.42E-01	1.32	0.62	6.5
p51		$k = a(R_{Hw})^n$	1.95E-02	0.49	0.57	6.8
p52		$k = a(R_{Bw})^n$	5.36E-02	0.47	0.63	6.4
p53		$k = a(R_{Hw_{ws}})^n$	9.95E-02	0.39	0.57	7.2
p54		$k = a(R_{Bw_{ws}})^n$	1.29E-01	0.41	0.63	6.6

571